

Stability of a Flying Wing UAV in Icing Conditions

Adrian Winter*[†], Richard Hann*, Andreas Wenz*, Kristoffer Gryte* and Tor Arne Johansen*
 *Norwegian University of Science and Technology
 7034 Trondheim, Norway
 adriawi@stud.ntnu.no · richard.hann@ntnu.no
[†]Corresponding author

June 2019

Abstract

An established reduced-frequency approach leveraging time-dependent 3D CFD-ALE simulations is used to calculate the static, quasi-static and dynamic stability derivatives of a clean and severely iced flying wing UAV at two angles of attack. Together with stationary 3D simulations, a quantitative assessment of changes to the flight behaviour can be made. The method can be used for any aircraft in any icing condition with minor limitations. The results show a severe degradation to some stability derivatives, especially in static longitudinal performance, whereas others are less affected and some even improved.

Nomenclature

Whenever possible, the symbols here are chosen in accordance with ISO1151 [1].

$(\cdot)_0$	Mean value	l, m, n	Roll, pitch, yaw moment
$(\cdot)_A$	Amplitude	p, q, r	Roll, pitch and yaw rate
α	Angle of attack (AOA)	S	(Wing) reference area
β	Angle of sideslip (AOS)	T_∞	Outside air temperature
ω	Oscillation frequency	u_b, v_b, w_b	Velocities in body-fixed x, y, z direction
θ	Pitch angle	V_a	Free stream velocity
ρ	Air density	ALE	Arbitrary Lagrangian-Eulerian
b	Wing span	CFD	Computational Fluid Dynamics
c	Chord	LWC	Liquid water content
c_M	Mean Aerodynamic Chord (MAC)	MVD	Median volume diameter
k_s	Surface roughness	UAV	Unmanned aerial vehicle
L, D, Y	Lift, drag and side force in air-path axes		

1. Introduction

During the last eighty years, there has been substantial research on icing of large aircraft [2–4]. Flying wings are also well understood [5] and have been used for decades in niche applications ranging from model airplanes to the strategic bomber *Northrop B-2 Spirit*. However, there is very little published research in icing of flying wings, especially at low Reynolds numbers. Before the advent of autonomous or at least radio controlled commercial flight of small aircraft, there has been little interest in investigating these icing effects on low-Reynolds aircraft: Commercial aviation has used manned aircraft with ice-protection systems, and hobbyists have little reason to fly in icing conditions, which

FLIGHT CHARACTERISTICS OF ICED UAV

are most commonly encountered in clouds. This study aims to close this gap by first describing a generic method to determine relevant aerodynamic properties with numeric simulations and then apply these methods to a medium-sized flying wing.

The issue of icing of unmanned aerial vehicles (UAV) has been known to researchers since at least the early 1990s [6], but has only recently been addressed. Given the ever-growing list of applications of UAVs, ranging from scientific and commercial applications such as aerial photography to governmental and military tasks such as border control, it is apparent that all-weather capabilities, including flight into suspected icing conditions, are of major concern. This especially applies to flight in cold climates such as the Arctic, but can also be a concern in moderate climates [7]. In consequence, if operation capabilities should not be limited, there are only two possibilities: either the small UAV needs to have a classical ice protection that is able to remove ice accretion [8] – or flight with iced wings has to be safely possible despite the severely degraded key flight characteristics such as maximum lift, drag, stall angle of attack (AOA) and stability [9, 10]. Since ice protection equipment may require structural changes and additional weight due to additional equipment and often consumes large amounts of energy, it may be advantageous to accept aerodynamic penalties in these situations and let the flight controllers handle the icing conditions to the degree possible, especially if icing only occurs occasionally. This knowledge could also enable a short-term icing severity forecast that could help in the decision to continue or abort a flight.

Recent accidents have shown that even in the 21st century, and with aircraft equipped with ice protection systems, icing remains a major concern. For example, there have been four losses of the ATR-72 alone between 1994 and 2012 that have icing as suspected cause or contributing factor [7, 11–13]. The US military has lost several aircraft in Afghanistan and had to withdraw UAVs from Hungary due to their inability to fly safely in these conditions [14, 15].

To develop autopilots or fly-by-wire-systems that are capable of flying with iced wings, it is necessary to know the static and dynamic behaviour of the entire aircraft with iced airfoils. However, the analytical or empirical methods of estimating the relevant factors all have limitations that make them inadequate for the problem:

Determining the static behaviour such as the pitch stability, i. e. the aircrafts tendency to return to equilibrium after a pitch perturbation, using CFD methods for an arbitrary geometry can be done with static simulations that are computationally cheap compared to time-dependent simulations. For this, simulating the airflow at a few (≈ 15) distinct values for the AOA (α) and angle of sideslip (AOS, β) is sufficient. The main challenge here is not to determine the changes in forces and moments to the iced airfoil, but to determine appropriate ice shapes using experiments in icing wind tunnels [10] or numerical tool such as FENSAP-ICE, LEWICE or others [16, 17].

Determining the dynamic behaviour such as damping, however, is not as simple: Etkin [18] lists several analytical methods to determine the quasi-static stability derivatives (i. e. those that depend on the roll-, pitch-, and yaw rates p, q, r), but these methods are only applicable for a very narrow set of conditions, such as attached airflow at zero AOA. This proves to be even more challenging for the dynamic derivatives (i. e. those that depend on $\dot{\alpha}$ and $\dot{\beta}$), where he only offers a method for estimating the $\dot{\alpha}$ derivatives for a thin sheet. Additionally, many analytical methods assume a tailed aircraft where the tail dominates the pitch and yaw behaviour.

XFLR5 is a software, originally developed for model airplanes, that is capable of estimating many aspects of small aircraft aerodynamics with decent accuracy [19, 20], but has severe limitations that make it unsuitable for iced calculations. See Sec. 3.1 for a discussion of XFLR in context of iced simulations.

For this reason, time-dependent numerical simulations have to be used for all quasi-static and dynamic derivatives. Building on the previous work from Murman [21] and its more practical, application-oriented realization by Schmidt and Newman [22], the decision has been made to use Computational Fluid Dynamics with Arbitrary Lagrangian-Eulerian methods (CFD-ALE) to simulate the dynamic behaviour and determine the derivatives using a simple curve fitting process implemented in MATLAB.

Dynamic experiments in wind tunnels are possible, but uncommon, difficult and expensive. This data was not available for the airframe that was used for the simulations here. Flight tests, an important part of every flight test programme for manned flight, are also possible. They always carry the risk of damaging the vehicle and therefore have to be done safely and carefully. They are more useful at the end of the development cycle to verify and certify the previous development. Flight test data with artificial ice shapes have been performed with the UAV used for the numerical simulations, but have not yet been evaluated in detail. For this reason, 2D results found in the literature [23] are used to verify the model proposed here.

Hann et al. have investigated three icing scenarios and the influence on UAV operations in a previous work [9]. Their study however used a 2D airfoil in a classic wing-and-tail configuration to extrapolate results that should be qualitatively, but not necessarily quantitatively correct. 2D simulations can not yield results for the lateral case. Additionally, only static investigations were performed and thus no dynamic derivatives included. The three ice formes used in that study were based on 14 CFR Part 25, App. C for maximum continuous icing [24]. Of these cases, the worst case – mixed ice – has been chosen in this study.

2. Methodology

2.1 Ice model and tools

There are three major classes of ice that form in icing conditions: glaze ice, rime ice and mixed ice [25]. Glaze ice forms at relatively high temperatures just below the freezing point and is characterized by a smooth, translucent ice cover that has relatively little influence on the airflow, but is dangerous due to the potentially very high growth rates and the potential of runback behind the leading edge, that can lead to blocked control surfaces in extreme cases. At the other end of the spectrum, i. e. at low temperatures below approximately minus five degrees Celsius, rime ice forms, which is characterized by a very rough, opaque surface, which has a stronger influence on airflow than glaze ice, but due to the low liquid water content of air at these temperatures, the growth rates of rime ice are typically low. For this reason, it is arguably the least dangerous icing condition.

The icing conditions with the largest impact on flight characteristics [9], that is the largest penalties on maximum lift, drag, pitch stability and stall angle, is mixed ice. This type forms at temperatures between glaze and rime, and is characterised by horn-like structures roughly 45° to the airflow that cause detachment bubbles and fully turbulent airflow. A cross section of the iced airfoil with clearly visible horns can be found in Fig. 2. This is a plot of the ice shape that was used in this work, as it is deemed the worst case. The environmental conditions that lead to this mixed ice condition were identical to the previous work by Hann et al. [9], and are repeated in Tab. 1. Note that the icing velocity $V_{a,icing}$ of 40 m/s is almost twice the typical cruise speed of the UAV. This speed was selected to obtain the distinct horn formation [16].

Within this work, it is assumed that ice only forms on the wings, so the body, propeller, and winglets are not affected by icing. This is clearly visible in Fig. 1, which shows the model of Skywalker X8 used for the simulations, as the red-shaded area.



Figure 1: Ice accretion on X8 model

Table 1: Values used for icing simulation

Property	Symbol	Value
Icing velocity	V_{icing}	40 m/s
Icing time	t_{icing}	40 min
Chord	c	0.3 m
Icing AOA	α_{icing}	0°
Median volume diameter	MVD	20 μm
Liquid water content	LWC	0.55 g/m ³
Outside air temperature	T_∞	-4°C
Surface roughness	k_s	1 mm

Table 2: Physical properties of X8

Property	Value
Takeoff mass	4 kg
Wing span	2.1 m
Mean aerodynamic chord	0.35 m
Airfoil	unspecified [26]
Cruise speed	≈ 20 m/s
Sweep at leading edge	$\approx 30^\circ$
Wing area (without body)	≈ 0.4 m ²
Wing reference area (defined)	0.75 m ²

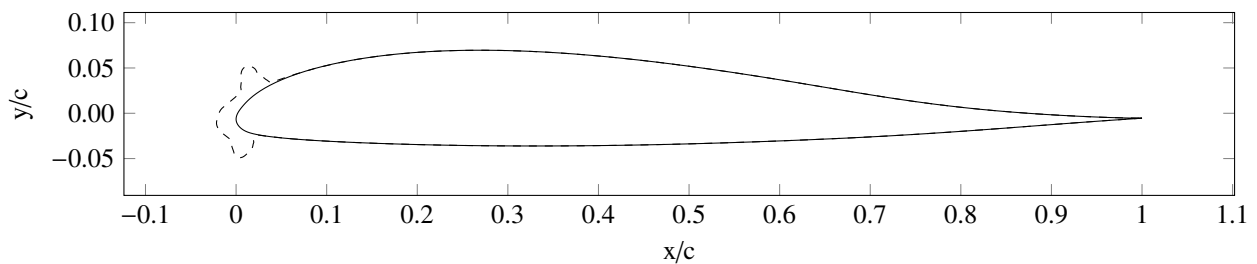


Figure 2: X8 cross section of the wing for the iced and clean configuration

This model is then discretized into a mesh using Pointwise, which is then used with the ALE method of FENSAP to generate time-dependent forces and moments. FENSAP is the flow solver [27] of the FENSAP-ICE toolbox that is developed by ANSYS Inc. To obtain the airflow solution, FENSAP solves the unsteady compressible Reynolds-

FLIGHT CHARACTERISTICS OF ICED UAV

averaged Navier Stokes (RANS) equations [28]. Turbulence is simulated by the either the Spalart-Allmeras or the $k - \omega - SST$ model.

FENSAP-ICE is a state-of-the-art toolbox that covers several aspects of icing in context of fluid dynamics: Amongst other things, FENSAP-ICE is able to simulate ice accretion, aerodynamic forces and moments, instationary effects and mesh deformation. In this study, only the flow solver FENSAP has been used. With the ALE toolbox, sinusoid oscillations around all three body-fixed axes (three rotations, three translations) can be simulated. This is done by moving the mesh relative to the flow [29].

After parsing the output files, the data is processed using MATLAB's curve fitting toolbox.

2.2 Flight mechanics model and curve fitting

The common [18, 26, 30, 31] flight mechanics model for rigid aircraft has been used in this work: This model assumes that the longitudinal parameters angle of attack α , pitch rate q and change of angle of attack $\dot{\alpha}$ have no influence on the side force Y , the roll moment l and the yaw moment n – and the lateral parameter angle of sideslip β , roll rate p , yaw rate r and change of angle of sideslip $\dot{\beta}$ have no influence on lift L , drag D and pitching moment m . All forces are given in the air-path fixed coordinate system, the moments in body-fixed axes.

$$L \approx \frac{1}{2} \rho V_a^2 S \cdot (C_L(\alpha) + C_{L_q} \frac{c_M}{2V_a} q + C_{L_{\dot{\alpha}}} \frac{c_M}{2V_a} \dot{\alpha}) \quad (1)$$

$$D \approx \frac{1}{2} \rho V_a^2 S \cdot C_D(\alpha) \quad (2)$$

$$m \approx \frac{1}{2} \rho V_a^2 S c_M \cdot (C_m(\alpha) + C_{m_q} \frac{c_M}{2V_a} q + C_{m_{\dot{\alpha}}} \frac{c_M}{2V_a} \dot{\alpha}) \quad (3)$$

$$Y \approx \frac{1}{2} \rho V_a^2 S \cdot (C_Y(\beta) + C_{Y_p} \frac{b}{2V_a} p + C_{Y_r} \frac{b}{2V_a} r + C_{Y_{\dot{\beta}}} \frac{b}{2V_a} \dot{\beta}) \quad (4)$$

$$l \approx \frac{1}{2} \rho V_a^2 S b \cdot (C_l(\beta) + C_{l_p} \frac{b}{2V_a} p + C_{l_r} \frac{b}{2V_a} r + C_{l_{\dot{\beta}}} \frac{b}{2V_a} \dot{\beta}) \quad (5)$$

$$n \approx \frac{1}{2} \rho V_a^2 S b \cdot (C_n(\beta) + C_{n_p} \frac{b}{2V_a} p + C_{n_r} \frac{b}{2V_a} r + C_{n_{\dot{\beta}}} \frac{b}{2V_a} \dot{\beta}) \quad (6)$$

In this set of equations, the model is linearized in all parameters except α and β , and the constant influence of B on A is given as *stability derivative* C_{A_B} . The p, q, r -derivatives are called the *quasi-static* derivatives, and the $\dot{\alpha}, \dot{\beta}$ -derivative *dynamic* derivatives. The quasi-static and dynamic derivatives are summarized to “instationary derivatives” within this paper. Note that the derivatives are assumed to be constant, i. e. $C_{L_q} \neq f(\alpha, \dot{\alpha}, q, \dots)$, which is *not* the case for the dynamic derivatives that are inherently dependent on the motion itself. However, for a given reduced frequency, these derivatives are useful nonetheless, e. g. for verification – see Sec. 3.2.

The model for drag is different than the model for all other forces and moments. It does not allow for determining the instationary derivatives. For a disussion of the reasons for this decision, see Sec. 5.3

There are slightly different ways to non-dimensionalize the coefficients, which usually differ by the used reference length and factors of two. The above notation was chosen because it is in line with the previous work of Gryte et al. [26]. Additionally, the wingspan b , the MAC c_M and the wing reference area S are the same, so the numerical results can be compared directly.

After linearization in α and β , these six equations are directly used for the curve fitting process, contrary to the approach Schmidt and Newman have used [22]. This removes the restrictions that the model can only be used for the longitudinal motion.

2.3 Determining the static behaviour

By running static CFD simulations, where the AOA and AOS are varied in steps of one to two degrees from low to high values and the resulting forces and moments are calculated, the static behaviour can be determined. This is often called a “AOA sweep” and “AOS sweep”, respectively. In case of the AOA this is done until stall, while for the AOS, 10° is seen as the maximum realistic value. The forces and moments determined at these static, discrete points, can then be used for the simulator using a simple interpolation. Additionally, the linearized model (e. g. $C_L(\alpha) \approx C_{L_\alpha} \alpha + C_{L_0}$) can be determined by a linear regression after the values that are clearly beyond the linear range (onset of stall) are removed.

2.4 Reduced frequency approach with a single oscillation (determining instationary derivatives)

Previous work by Murman [21] has shown that determining the system response to a single reduced frequency is often precise enough and much less computationally expensive than a full time-dependent simulation which attempts to resolve all frequency modes. *Reduced frequency* refers to a non-dimensionalized frequency

$$k = \frac{\omega c}{2V_a} \quad (7)$$

with the oscillation frequency ω , the chord c (in two-dimensional cases c , in three-dimensional cases the mean aerodynamic chord (MAC) c_M is used instead) and the free stream velocity V_a . This number serves as a measurement of the “unsteadiness” of the problem. The model from Eq. (1) to Eq. (6) is only valid for $0 < k \ll 1$ [18].

The aircraft’s flight on the desired trajectory is simulated, and the aircraft’s response is calculated. This is similar to wind tunnel tests, where the aircraft is fixed “on rails”, and the outside forces and moments that are applied to the structure are measured. Note that the control surfaces are in neutral position all the time and not used to generate the necessary flight paths, and therefore the control derivatives are not determined.

The linearized flight model from Sec. 2.2 has three ($\alpha, \dot{\alpha}, q$ -derivatives) or four ($\beta, \dot{\beta}, p, r$ -derivatives) degrees of freedom, respectively, but the forced oscillation only two (the motion itself and its derivative). For this reason, there is a linear dependency between the parameters determined by the curve fitting. By choosing the flight path as described in Sec. 2.4.1 and 2.4.2, this linear dependency can be resolved and all 15 instationary derivatives can be determined. The curve fitting also determines the linearized static behaviour (e. g. $C_L(\alpha) \approx C_{L_0} + C_{L_\alpha}\alpha$), but this can be more easily and more precisely determined by the α and β sweep as described in Sec. 2.3.

When forced into an oscillation, the resulting forces and moments will have a phase lag δ compared to the exciting function, as can be seen in Fig. 3. This phase lag of a few degrees is determined in the curve fitting process and contains the information about the instationary stability derivative. For this to work, the resulting force must be linearly dependent on the exciting function: $C_L = m \cdot \alpha(t) + n \cdot \dot{\alpha}(t)$. This is the reason why local linearity is a necessary precondition for this model to work. Local linearity means that the deviation between the linear model and the numerical results in the oscillation interval (for example $\alpha_0 \pm \alpha_A$) must be low. In other words the curvature of the corresponding function (for example at $C_L(\alpha_0)$) must be low.

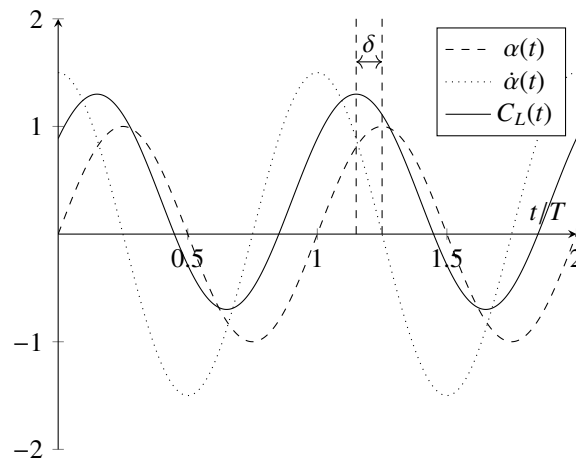


Figure 3: Exaggerated illustration of the Schmidt and Newman-approach

In the following descriptions a pure sine exciting function is assumed. All oscillations have a mean value (e. g. α_0), an amplitude (e. g. α_A), and a frequency ω , so for the AOA the exciting function would be $\alpha(t) = \alpha_0 + \alpha_A \sin(\omega t)$.

2.4.1 Test cases – longitudinal

The three parameters in the longitudinal motion are $\alpha, \dot{\alpha}, q$, which can be changed by either a pitching motion (i. e. changing the pitch angle θ), or a translational plunging motion around the aircraft’s body-fixed z -axis.

To increase readability, the following section only lists the equations for lift. The equations are analogous for the pitching moment.

These three cases are illustrated in Fig. 4. Note that in the first and third case, a mean AOA of zero degrees is illustrated – this is a special case: both cases can have a nonzero mean AOA. The blue arrows indicate the air stream

FLIGHT CHARACTERISTICS OF ICED UAV

velocity, the red arrows the body-fixed x-axis and the grey dotted line the flight path. The angle between the red and blue arrows is the AOA.

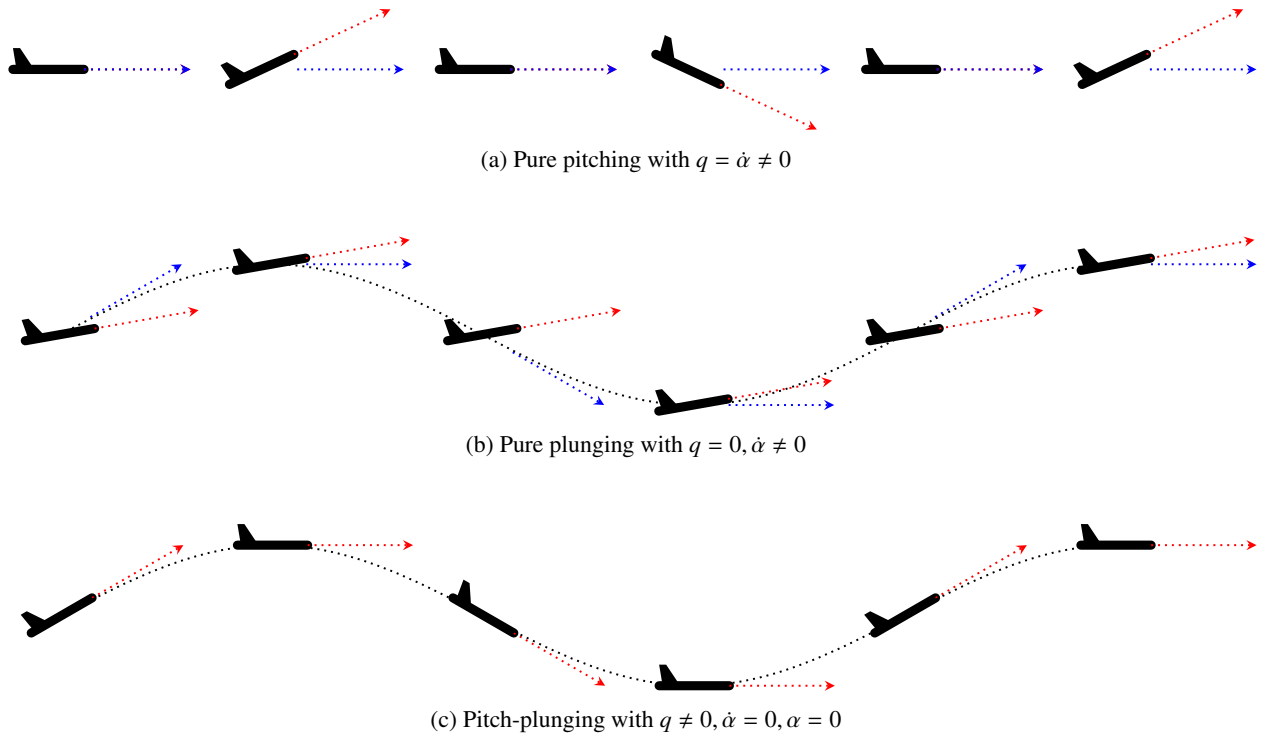


Figure 4: Illustration of the three longitudinal flight paths

Case a: Pure pitching motion In this case, the aircraft pitches on a horizontal flight path without changes in flight altitude/vertical velocity.

$$\theta(t) = \alpha(t) = \alpha_0 + \alpha_A \cdot \sin(\omega t) \quad (8)$$

$$\Rightarrow q = \dot{\theta} = \alpha_A \cdot \omega \cdot \cos(\omega t) \quad (9)$$

$$\Rightarrow \dot{\alpha} = \alpha_A \cdot \omega \cdot \cos(\omega t) \quad (10)$$

From comparing Eq. (9) and (10), it is obvious that $\dot{\alpha} = q$. Therefore only a combined damping derivative $C_{L_{\text{damp}}}$ can be determined:

$$C_L(t) \approx C_{L_0} + C_{L_\alpha} \alpha(t) + C_{L_q} \frac{c}{2V_a} q(t) + C_{L_{\dot{\alpha}}} \frac{c}{2V_a} \dot{\alpha}(t) \quad (11)$$

$$C_L(t) \approx C_{L_0} + C_{L_\alpha} \cdot \alpha(t) + \underbrace{(C_{L_q} + C_{L_{\dot{\alpha}}})}_{C_{L_{\text{damp}}}} \frac{c}{2V_a} \dot{\alpha}(t) \quad (12)$$

$$C_L(t) \approx C_{L_0} + C_{L_\alpha} \cdot (\alpha_0 + \alpha_A \sin(\omega t)) + C_{L_{\text{damp}}} \underbrace{\frac{c}{2V_a} \omega \alpha_A \cos(\omega t)}_k \quad (13)$$

Since $C_{L_{\text{damp}}}$ is assumed to be constant, the phase difference δ between the exciting function and the system response is directly dependent on k . Choosing a too low value of k for the simulations therefore results in a very small phase lag that is difficult to resolve in the fit. Choosing a too high value of k violates the assumption of the model ($k \ll 1$) and leads to wrong results.

Case b: Pure plunging motion In this case, the pitch angle θ is kept constant, and the AOA $\alpha = \arcsin(w_b/V_a) \approx w_b/V_a$ is varied by changing the vertical velocity.

$$\theta(t) = \theta_0 \quad (14)$$

$$\alpha(t) = \frac{w_A}{V_a} \cdot \sin(\omega t) = \alpha_{A,\text{equiv.}} \cdot \sin(\omega t) \quad (15)$$

$$\Rightarrow q = 0 \quad (16)$$

$$\Rightarrow \dot{\alpha} = \alpha_{A,\text{equiv.}} \cdot \omega \cdot \cos(\omega t) \quad (17)$$

Therefore, the q -derivative is undefined and only the $\dot{\alpha}$ -derivative is determined:

$$C_L(t) \approx C_{L_0} + C_{L_\alpha} \cdot \alpha(t) + C_{L_{\dot{\alpha}}} \frac{c}{2V_a} \dot{\alpha}(t) \quad (18)$$

Case c: Combined pitching and plunging motion In this case, the AOA is kept constant by plunging down when the UAV is pitched down. The plunging velocity is chosen such as that the increase in AOA from the down-motion is equal to the decrease of AOA from the pitch down-motion – and vice versa.

$$\theta(t) = \theta_0 + \theta_A \sin(\omega t) \quad (19)$$

$$w(t) = w_A \sin(\omega t) \Rightarrow \alpha_{\text{equiv.}}(t) = \alpha_{A,\text{equiv.}} \cdot \sin(\omega t) \quad (20)$$

$$\Rightarrow \alpha(t) = \alpha_0 + \underbrace{(\theta_A + \alpha_{A,\text{equiv.}})}_{=0} \sin(\omega t) \quad (21)$$

$$\Rightarrow q = \theta_A \omega \cos(\omega t) \quad (22)$$

In this case, the AOA is kept constant, which means that the terms C_{L_0} and $C_{L_\alpha} \alpha$ are linearly dependent and cannot be determined by the curve fitting process. Only the q -derivative can be determined.

$$C_L(t) = \underbrace{C_{L_0} + C_{L_\alpha} \alpha}_{\text{const.}} + C_{L_q} \frac{c}{2V_a} q(t) \quad (23)$$

2.4.2 Test cases – lateral

The lateral test cases are very similar to the longitudinal cases, except in all cases the mean AOS is zero ($\beta = 0$), and that there are four properties/derivatives for each of the three forces and moments. Only the exciting functions are given here, and the side force Y is used as place holder for the roll moment l and yaw moment n . A sideways motion (equivalent to the plunging described above) is called “traversal” in this paper. For symmetry reasons, the constant factors C_{Y_0} , C_{l_0} , C_{n_0} should all be zero. To improve the curve fitting process, these factors are included in the model, but the numerical values determined by the fit are always very small.

Case d: Pure Yawing In this case, the AOS is time-dependent and the yaw rate is equal to the change in AOS $\dot{\beta}$. Similar to case a, only a combined derivative $C_{Y_{\text{damp}}} = C_{Y_\beta} + C_{Y_r}$ can be determined.

$$\beta(t) = \beta_A \sin(\omega t) \quad (24)$$

$$\dot{\beta}(t) = \beta_A \omega \cos(\omega t) \quad (25)$$

$$r = \dot{\beta}(t) \quad (26)$$

$$C_Y(t) = C_{Y_0} + C_{Y_\beta} \beta(t) + C_{Y_{\text{damp}}} \frac{b}{2V_a} \dot{\beta}(t) \quad (27)$$

Case e: Pure Traversal In this case, the AOS is time dependent, and the yaw rate is zero. With the side-velocity amplitude v_A , the equivalent AOS is $\beta_{A,\text{equiv.}} \approx v_A/V_a$

$$\beta(t) = \beta_{A,\text{equiv.}} \sin(\omega t) \quad (28)$$

$$\dot{\beta}(t) = \beta_{A,\text{equiv.}} \omega \cos(\omega t) \quad (29)$$

$$r = 0 \quad (30)$$

$$C_Y(t) = C_{Y_0} + C_{Y_\beta} \beta(t) + C_{Y_{\dot{\beta}}} \frac{b}{2V_a} \dot{\beta}(t) \quad (31)$$

FLIGHT CHARACTERISTICS OF ICED UAV

Case f: Yawing and traversal In this case, the AOS is zero, and the yaw rate is nonzero

$$\beta(t) = \dot{\beta} = 0 \quad (32)$$

$$r(t) = \beta_A \omega \cos(\omega t) \quad (33)$$

$$C_Y(t) = C_{Y_0} + C_{Y_r} \frac{b}{2V_a} r \quad (34)$$

Case g: Pure rolling In this case, the AOS is zero, and the roll-rate is time-dependent.

$$\beta(t) = \dot{\beta} = 0 \quad (35)$$

$$p(t) = p_A \omega \cos(\omega t) \quad (36)$$

$$C_Y(t) = C_{Y_0} + C_{Y_p} \frac{b}{2V_a} p \quad (37)$$

3. Validation of the instationary results

There is no suitable experimental data from the Skywalker X8 available to directly compare the results from the simulations to. Therefore, to validate the methodology, three different indirect approaches were employed:

- Comparison with XFLR5 and wind tunnel, where available
- Check of internal consistency
- Comparison with 2D test cases from the literature

None of these approaches yield a definite proof that the proposed method and results are adequate, but taken together they may offer a strong indication that the results are accurate.

Lacking the required experimental data, the lateral results can only be checked for internal consistency and compared with the XFLR5 results. However, Murman has already shown in [21], that the method works for the lateral derivatives. It is therefore assumed that if the longitudinal verification is successful, the method also works in the lateral case.

3.1 Comparison with XFLR5 results

Gryte et al. [26] have already compared the XFLR5 results to the wind tunnel data, where it was shown that the static XFLR5 results are reasonable, but an assessment of the instationary XFLR5 results was not possible with the available data. The XFLR5 calculations are listed together with the results of this work in the tables in the next section. No attempt of a quantitative comparison with XFLR5 is made, because the XFLR5 results themselves have severe limitations. The methods used by XFLR5 work reasonably well for the clean case and simple geometries [19, 20], but fail to deliver accurate results in more complex cases [32]. The XFLR5 documentation does not go into detail how the quasi-stationary stability derivatives are determined, but explicitly states that “the potential flow model is only valid in conditions of limited flow separation” [33], an condition that is violated in the iced case. XFLR5 also generally is limited to simple geometries and for example is unable to accurately predict a wing-body intersection or large control surface deflections. Last, XFLR5 tends to under-estimate drag even in ideal conditions. In summary, trying to simulate icing would violate almost all recommendations mentioned in the XFLR5 manual [33].

3.2 Check of internal consistency

Two main checks were done: verification of the sample rate (i. e. unsteady CFD time step) and verification of the damping sums. The sample rate was increased from about 20 samples per period to 1000 samples per period. The results from 20 samples per period differed from the other results by less than 5%, and more than 100 samples per period did not significantly alter the results, see Tab. 3. For this reason, 100 samples per period was chosen as a compromise between computational complexity and precision. The test case is equivalent to the low AOA clean test case from the previous section.

For the test cases a-f, the internal consistency can also be checked. This means, that the results from the pure pitching/yawing cases should be the sum of the other instationary derivatives. Table 4 and 5 list the results of the longitudinal comparison. The agreement is good, except for the high AOA clean cases, which might be caused by large non-linearities due to the onset of flow separation at 8° AOA.

Table 3: Comparison between the dynamic derivatives for different sample rates

Case	Samples (1/T)	$C_{L_{damp}}$	Δ	$C_{m_{damp}}$	Δ
Sample rate 1	50	2.52	-5.62%	-1.38	-3.50%
Sample rate 2	100	2.63	-1.50%	-1.42	-0.70%
Sample rate 3	200	2.66	-0.37%	-1.43	0.00%
Sample rate 4	500	2.67	–	-1.43	–

Table 4: Comparison of directly determined (“damp”) and summed (“sum”) lift derivatives

Case	C_{L_q}	$C_{L_{\dot{\alpha}}}$	$C_{L_{damp}}$	$C_{L_{sum}}$	ΔC_L
X8 Clean Low AOA	4.64	-1.89	2.63	2.75	-0.12
X8 Clean High AOA	4.60	-0.25	2.89	4.35	-1.46
X8 Iced Low AOA	-3.31	3.27	0.21	-0.04	0.25
X8 Iced High AOA	-3.51	5.43	2.24	1.92	0.32

Table 5: Comparison of directly determined (“damp”) and summed (“sum”) pitching moment derivatives

Case	C_{m_q}	$C_{m_{\dot{\alpha}}}$	$C_{m_{damp}}$	$C_{m_{sum}}$	ΔC_m
X8 Clean Low AOA	-1.99	0.63	-1.31	-1.36	0.06
X8 Clean High AOA	-0.28	-1.35	-1.50	-1.63	0.13
X8 Iced Low AOA	-2.00	-0.64	-2.65	-2.64	-0.01
X8 Iced High AOA	-2.12	1.13	-0.99	-0.98	0.01

3.3 Two dimensional verification simulations

In the 1970s and 80s, investigations in the dynamic behaviour of helicopter blades has been made and summarized in the AGARD-R-702 report [23]. For the verification here, two-dimensional results with the symmetric laminar flow airfoil NACA 64_A010 were chosen. These cases have the AGARD-IDs “DI7” and “DI29”. Of all two dimensional airfoil experiments, these two cases were the closest to the problem at hand in Mach number. The two 2D cases were simulated with the unsteady ALE approach in FENSAP for for longitudinal movements as decribed above (Case a). The test parameters are listed in Tab. 6, and the results in Tab. 7.

The results show good agreement for the dynamic derivatives ($C_{L_{dyn,AGD}} \approx C_{L_{dyn,CFD}}$ and $C_{m_{dyn,AGD}} \approx C_{m_{dyn,CFD}}$), but poor agreement for the static pitch derivative $C_{m_{\dot{\alpha}}}$. This value should theoretically be close to zero in both cases: In subsonic flow the neutral point is approximately at 25% c, and characterized by a pitching moment that is almost independent of the AOA. The reason for the differences could not be determined. Possible explanations include simulation errors, for example caused by transition issues, and measurement errors in the report. During the AGARD experiments, the forces and moments were derived from the pressure distribution instead of being measured directly.

The method is only used to determine instationary results, where the agreement is good. Nonetheless, further verification simulations that aim to resolve the disagreement, should be considered.

FLIGHT CHARACTERISTICS OF ICED UAV

Table 6: Properties used in verification simulations

Property	CT 1 (DI 7)	CT 2 (DI 29)
Profile	NACA 64 _A 010	NACA 64 _A 010
Chord	0.5 m	0.5 m
Frequency	10.4 Hz	10.8 Hz
Mach-number	0.490	0.502
α_0	-0.01°	-0.22°
α_A	0.96°	1.02°
Rotation axis	0.233 x/c	0.269 x/c
Moment ref. axis	0.25 x/c	0.25 x/c
Reynolds-number	$2.52 \cdot 10^6$	$9.98 \cdot 10^6$
Transition	Free	Free

Table 7: Comparison between AGARD results and CFD-ALE simulations)

Test Case	k	$C_{L_\alpha,AGD}$	$C_{L_\alpha,CFD}$	$C_{L_{dyn},AGD}$	$C_{L_{dyn},CFD}$	$C_{m_\alpha,AGD}$	$C_{m_\alpha,CFD}$	$C_{m_{dyn},AGD}$	$C_{m_{dyn},CFD}$
CT 1 (DI7)	0.1	6.139	5.75	-11.49	-9.45	0.165	-0.10	-1.36	-1.45
CT 2 (DI29)	0.1	6.163	5.68	-10.36	-9.42	0.167	-0.10	-2.01	-1.17

4. Results

Simulations were conducted using the existing UAV platform at the NTNU UAVlab, which is a *Skywalker X8* medium-sized flying wing with swept wings and relatively large winglets that also serve as a vertical stabilizer. Some physical properties are listed in Tab. 2. The aircraft has no rudder, which means that the yaw stability is of very high concern, as electronic yaw compensation is not possible.

4.1 Static Behaviour

Results from the AOA and AOS sweeps as described in Sec. 2.3 can be found in Fig. 5. Only the sweeps for the decoupled model, i. e. without the influence of β on L, D, m , are plotted. Tab. 8 lists the linearized parameters (except for drag) for small α and β , where for example $C_L(\alpha) \approx C_{L_\alpha}\alpha + C_{L_0}$ with α in radians.

4.2 Instationary behaviour

All simulations have been conducted with an amplitude of 2° and a frequency of 2 Hz, which is equivalent to $k = 0.13$ at a free stream velocity of 17 m/s for the given geometry with $c_M = 0.35$ m. All simulations have been performed at a low AOA of 2°, and a high AOA of 8°, which is close to the stall angle for the iced case. The curve fitting also determines static derivatives, but these are not listed because the sweeps from the previous section is more precise. The XFRL5 data is, where available, listed and taken from Gryte et al. [26].

Table 8: Parameters for linearizations of AOA and AOS dependencies

Function	Linear factor clean	Constant factor clean	Linear factor iced	Constant factor iced
$C_L(\alpha)$	4.06	0.03	3.26	0.01
$C_m(\alpha)$	-1.00	0.00	-0.83	0.00
$C_Y(\beta)$	0.16	0.00	0.17	0.00
$C_l(\beta)$	-7.6×10^{-2}	0.00	-6.5×10^{-2}	0.00
$C_n(\beta)$	2.2×10^{-2}	0.00	2.6×10^{-2}	0.00

FLIGHT CHARACTERISTICS OF ICED UAV

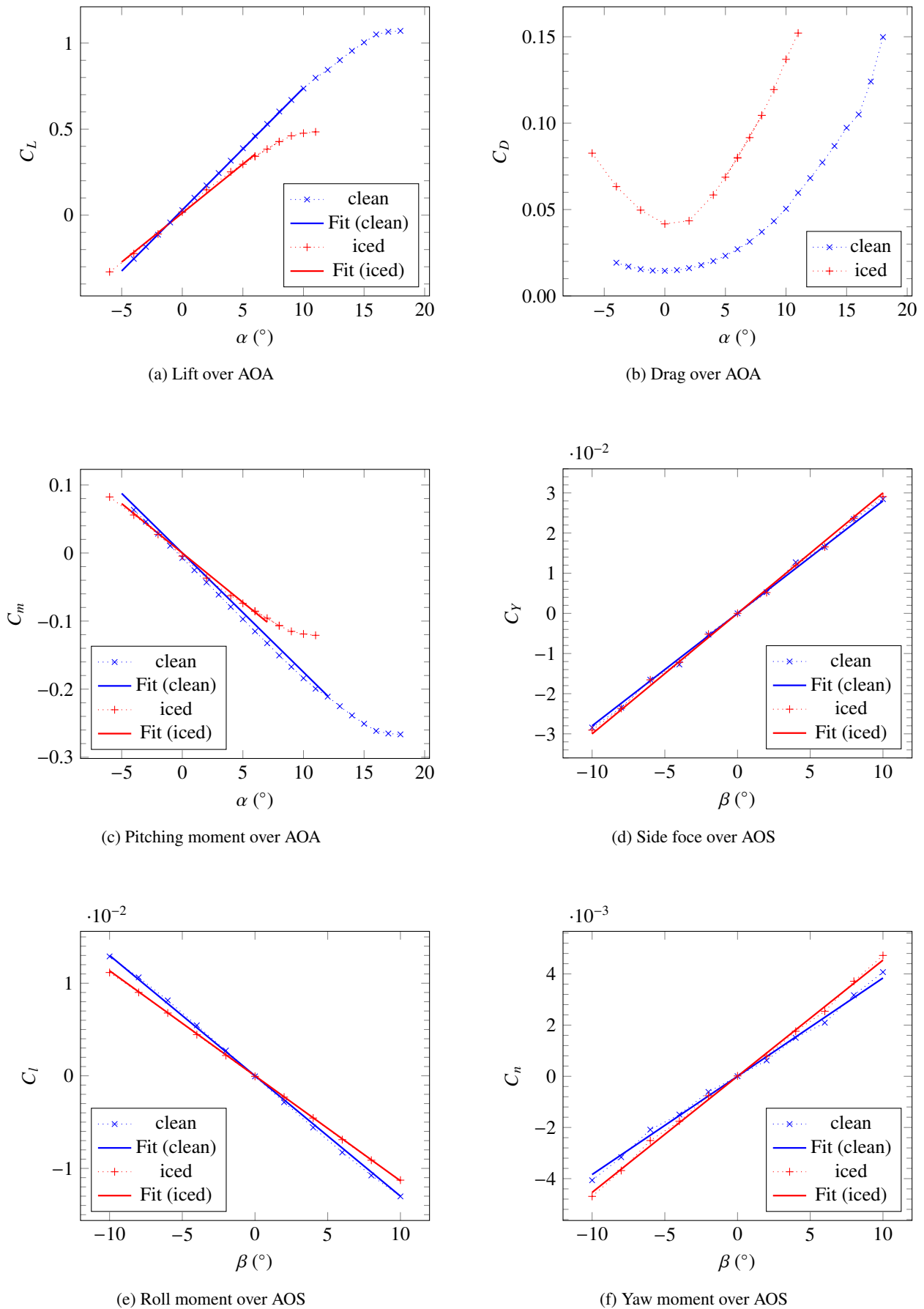


Figure 5: Static longitudinal and lateral behaviour, clean and iced. Parameters of fitted curves in Tab. 8

FLIGHT CHARACTERISTICS OF ICED UAV

Table 9: Comparison of the longitudinal derivatives at all four points

Derivative	Clean Low AOA	Iced Low AOA	Clean High AOA	Iced High AOA	XFLR5
C_{L_q}	4.64	-3.31	(4.60)	-3.51	3.87
$C_{L_{\dot{\alpha}}}$	-1.89	3.27	(-0.25)	5.43	
$C_{L_{\text{dyn}}}$	2.65	0.20	2.89	2.24	
C_{m_q}	-2.00	-2.00	(-0.29)	-2.12	-1.3
$C_{m_{\dot{\alpha}}}$	0.63	-0.63	(-1.35)	1.13	
$C_{m_{\text{dyn}}}$	-1.32	-2.65	-1.50	-0.99	

Table 10: Comparison of all instationary lateral derivatives

Derivative	Clean	Iced	XFLR5
$C_{Y_{\beta}}$	-0.023	-0.034	
C_{Y_p}	-0.185	-0.133	-0.137
C_{Y_r}	0.005	0.002	0.084
$C_{Y_{\text{dyn}}}$	-0.042	-0.038	
$C_{l_{\beta}}$	0.028	0.123	
C_{l_p}	-0.409	-0.407	-0.404
C_{l_r}	0.039	0.158	0.056
$C_{l_{\text{dyn}}}$	-0.010	-0.026	
$C_{n_{\beta}}$	-0.011	-0.029	
C_{n_p}	0.027	0.017	0.004
C_{n_r}	-0.022	-0.049	-0.012
$C_{n_{\text{dyn}}}$	0.011	0.018	

5. Discussion

5.1 Static behaviour

The illustrations in Fig. 5 clearly show a severe degradation especially in lift and drag, where drag roughly triples at most AOAs, and the maximum lift coefficient is reduced by about 50% from 1.1 at 18° to 0.48 at 11°. At a moderate AOA of 4°, the drag coefficient increases from 0.02 to 0.05, at a high AOA of 10° C_D increases from 0.05 to 0.14. This result is very similar to the 2D-simulations from Hann et al. [9].

The side force is virtually unaffected by icing, which can be explained by the winglets not having ice accretion in the model. The different slopes in Fig. 5 (d) are within rounding error range. The roll stability $C_l(\beta)$ is slightly reduced, but the yaw/weathercock stability $C_n(\beta)$ is actually *increased*. The reason for this could be that due to the wing's sweep, the forward facing wing has a larger drag than the rearward wing – and with iced wings, this difference between the leading and trailing wing is amplified, leading to a higher yaw stiffness. X8 has no rudder, so a high yaw stiffness is very positive, because the inevitable side slip after an aileron input is then reduced sooner.

5.2 Instationary behaviour

The longitudinal results as presented in Tab. 9 are inconclusive. They show no clear correlation between clean and iced, nor between low and high AOAs. For the important pitch damping derivative C_{m_q} , we see that the iced cases and the low AOA clean case are very similar. The high AOA case shows nonlinear behaviour and thus a poor curve fit, so this data is unreliable. The values determined by a fit with a low R^2 -value are written in parentheses.

The large changes in the quasi-static lift derivative C_{L_q} from the clean to the iced case may be explained by the fact that the additional lift that would ordinarily be generated by the warped airflow with a pitch rate can not be delivered anymore. A partial stall with the corresponding decrease in lift could be a consequence and would explain the negative lift derivative.

The lateral results, all determined at a low AOA, partially can be well explained, and partially are more surprising. For example, the increase in C_{n_r} can probably be easily explained: During a yawing motion, the slower, inner wing

has less drag due to the lower dynamic pressure. Since the difference in drag is higher for the iced wing, this results in a yawing moment that reduces the yaw rate and tries to return the two wings to equilibrium. In contrast, the increase in yaw-rate induced roll C_{l_r} is more surprising. The slower, inner wing produces less lift due to the lower dynamic pressure and a roll moment is the result. According to Etkin [18], this roll moment is proportional to C_L in undisturbed flight, a factor that is slightly decreased for the wing at $\alpha = 2^\circ$.

A higher (absolute) value of the derivatives is not necessarily better, for example an excessive damping could also lead to sluggish flight behaviour. For this reason, no attempt of a qualitative assessment of the instationary derivatives is made here, and the consequences of changes to the instationary derivatives should be investigated using flight simulations with and without changes to the controllers. The importance of these derivatives also depends on the flight platform. For example, a high yaw rate induced roll moment (C_{l_r}) may be desired in a plane without ailerons where the bank angle only is a result of rudder input – whereas in typical tailed aircraft with ailerons and rudder such behaviour might be not desired because compensation with ailerons is required in stationary curved flight.

5.3 Instationary drag

As already mentioned, the model fails when trying to determine the dynamic drag influences. The reason for this is that, even at small AOAs, drag is very non-linear so that the linearized model as shown above does not apply. Several attempts to model the drag using the induced-drag formula, two of which are shown below, were made. This formula assumes a non-lift dependent drag (parasitic drag, C_{D_p} , signified with a capital P and not to be confused with the drag caused by roll rate C_{D_p}) and a lift-dependent drag (induced drag, C_{D_i}).

$$C_D(\alpha) \approx C_{D_p} + C_{D_i} = C_{D_p} + \frac{C_L^2(\alpha)}{\pi e_0 \Lambda} \quad (38)$$

$$\approx C_{D_p} + \frac{(C_{L_\alpha} \alpha + C_{L_0})^2}{\pi e_0 \Lambda} \quad (39)$$

$$\approx C_{D_p} + \frac{(C_{L_\alpha} \alpha + C_{L_0} + C_{L_q} \frac{c}{2V_a} q + C_{L_{\dot{\alpha}}} \frac{c}{2V_a} \dot{\alpha})^2}{\pi e_0 \Lambda} \quad (40)$$

The model equations (Eq. (39) and (40)) were then introduced instead of $C_D(\alpha)$ into Eq. (2). None of the variations yielded usable fits for the dynamic drag. In every case, either the fit was poor or the determined values deemed as highly unlikely. Additionally, there is no established model for dynamic drag, and the dynamic drag is usually neglected [18, 31] because its influence is assumed to be minor. The changes in drag caused by the dynamic effects, even if they had non-negligible values, also have little impact on flight characteristics as long as enough engine thrust is available. For this reason, the decision has been made not to attempt to determine values for C_{D_q} and $C_{D_{\dot{\alpha}}}$.

6. Further work

Most discrepancies can likely be explained by non-linearities in the simulations. For this reason, investigating the effects with other parameters that reduce the non-linearities, may be advised. For example, lower oscillation amplitudes, or different mean AOAs could lead to clearer results. Using a finer discretization in the parameters $\omega, \alpha_0, \alpha_A, k, \dots$ could yield hints to model restrictions and correlations between the parameters. This can easily be done with this model since only a few restrictions in these parameters are required to guarantee the model assumptions.

Alternatively, the demands for linear behaviour in α and β can possibly be relaxed by changing the fitted model function from the linearized function (11) to the semi-linearized model (1) with the results from the static sweeps. This may increase the quality of the results, especially for high-AOA-cases and for drag at all AOAs.

Further work that investigates the impact on the flight behaviour caused by the changes to the derivatives is already planned. For this, an existing flight simulator is modified to incorporate the results from this work. Afterwards, flight tests with 3D-printed artificial ice shapes are desirable to verify the results in real flight conditions.

To improve the flight simulations, the control derivatives, i. e. the system response to control surface input, should also be investigated. It may be interesting to investigate the influence of other ice shapes and on different aircraft configurations (particularly conventional tailed aircraft). For the flight simulators, it would be advantageous to have some continuous icing model that uses an appropriate interpolation between the investigated points. This could then be included in other applications such as the observer based icing detection system by Seron et al. [34]. For this, it is likely necessary to investigate influences of the parameters on the results further.

7. Conclusion

In this work, a previously established and validated method to determine quasi-static and dynamic stability derivatives using time-dependent CFD-ALE simulations was used to determine the instationary behaviour of a severely iced flying wing at low Reynolds numbers. Together with new stationary 3D simulations, this allows a quantitative assessment of changes to flight characteristics compared to the clean case. The method is generic and can be applied to all aircraft and icing conditions at almost all points in the flight envelope.

The model was validated once more against 2D test cases found in the literature. It has a high internal consistency if the model limitations are met. Therefore, even without experimental comparisons, there are strong indications that the model is adequate.

The results show a clear deterioration of static longitudinal flight performance, smaller but noticeable changes in the static lateral characteristics, and significant changes in some instationary properties. This data forms a basis to investigate changes to the flight properties of the full aircraft in severe icing conditions using a flight simulator and could be used in future for applications such as icing-tolerant autopilots or electronic in-flight icing detection.

8. Acknowledgments

The first author would like to thank the European Union for supporting this work that was done as part of a master's thesis via the Erasmus+ programme.

The author would also like to thank Dr. Werner Grimm from the Institute of Flight Mechanics and Control (iFR) at the University of Stuttgart, who has agreed to supervise him during his master's thesis.

The research was funded by the Norwegian Research Council (project no. 223254) through the NTNU Centre of Autonomous Marine Operations and Systems (NTNU AMOS) at the Norwegian University of Science and Technology, and partially by CIRFA grant number 237906.

References

- [1] ISO. ISO 1151-1:1988 – Flight dynamics – Concepts, quantities and symbols – Part 1: Aircraft motion relative to the air. Technical report, 1988.
- [2] Thomas P. Ratvasky, Judith Foss Van Zante, and J. T. Riley. NASA/FAA Tailplane Icing Program Overview (AIAA-99-0370). Technical report, 1999.
- [3] Frank T Lynch and Abdollah Khodadoust. Effects of ice accretions on aircraft aerodynamics. *Progress in Aerospace Sciences*, 37(8):669–767, 2001.
- [4] C. Deiler and T. Kilian. Dynamic aircraft simulation model covering local icing effects. *CEAS Aeronautical Journal*, 9(3):429–444, 2018.
- [5] Karl Nickel and Michael Wohlfahrt. *Tailless Aircraft in theory & practice*. Butterworth Heinemann, 1992.
- [6] R. A. Siquig. Impact of Icing on Unmanned Aerial Vehicle (UAV) Operations. Technical report, Naval Environmental Prediction Research Facility, 1990.
- [7] Aviation Safety Network (ASN). ASN Aircraft Accident ATR 72-212 CU-T1549. <https://aviation-safety.net/database/record.php?id=20101104-0> (accessed 2019-06-18).
- [8] Richard Hann, Kasper Borup, Artur Zolich, Kim Sorensen, Håvard Vestad, Martin Steinert, and Tor Johansen. Experimental Investigations of an Icing Protection System for UAVs. In *SAE Technical Paper*. SAE International, 2019.
- [9] Richard Hann, Andreas Wenz, Kristoffer Gryte, and Tor Arne Johansen. Impact of Atmospheric Icing on UAV Aerodynamic Performance. In *Workshop on Research, Education and Development of Unmanned Aerial Systems (RED-UAS)*, Linköping, 2017.
- [10] Richard Hann. UAV Icing: Ice Accretion Experiments and Validation. In *SAE Technical Paper*. SAE International, 2019.
- [11] Aviation Safety Council. Transasia GE 791 Occurrence Investigation Report. Technical report, 2002.

- [12] National Transportation Safety Board (NTSB). Aircraft Accident Report: American Eagle Flight 4184. Technical report, 1996.
- [13] Interstate Aviation Committee. Final report on results of investigation of accident (VP-BYZ). Technical report, 2013.
- [14] Dr. Daniel L. Haulman. U.S. Unmanned Aerial Vehicles in Combat, 1991-2003, 2003.
- [15] Lindamae Peck, Charles C. Ryerson, and C. James Martel. Army Aircraft Icing (ERDC/CRREL TR-02-13). Technical report, US Army Corps of Engineers – Cold Regions Research and Engineering Laboratory, 2002.
- [16] Richard Hann. UAV Icing: Comparison of LEWICE and FENSAP-ICE for Ice Accretion and Performance Degradation. *2018 Atmospheric and Space Environments Conference*, pages 1–8, 2018.
- [17] K Szilder and W Yuan. In-flight icing on unmanned aerial vehicle and its aerodynamic penalties. *Progress in Flight Physics*, 9:173–188, 2017.
- [18] Bernard Etkin and Lloyd Duff Reid. *Dynamics of Flight*. John Wiley & Sons, Inc., 1996.
- [19] Kristofer Gryte, Richard Hann, Mushfiqul Alam, Jan Rohac, Tor Arne Johansen, and Thor I. Fossen. Aerodynamic modeling of the Skywalker X8 Fixed-Wing Unmanned Aerial Vehicle. *2018 International Conference on Unmanned Aircraft Systems, ICUAS 2018*, pages 826–835, 2018.
- [20] A Deperrois. Modal analysis and experimental validation. Technical report, 2011.
- [21] Scott M. Murman. Reduced-Frequency Approach for Calculating Dynamic Derivatives. *AIAA Journal*, 45(6):1161–1168, 2007.
- [22] Stefan Schmidt and Daniel M Newman. Estimation of Dynamic Stability Derivatives of a Generic Aircraft. *17th Australasian Fluid Mechanics Conference (AFMC)*, 2010.
- [23] NATO Advisory Group for Aerospace Research and Development (AGARD). AGARD-R-702 - Compendium of Unsteady Aerodynamic Measurements. Technical report, NATO, 1982.
- [24] Federal Aviation Administration. Part I – Atmospheric Icing Conditions. 14 CFR 25 Appendix C, 2011.
- [25] R. W. Gent, N. P. Dart, and J. T. Cansdale. Aircraft icing. *Philosophical Transactions of the Royal Society A: Mathematical, Physical and Engineering Sciences*, 358(1776):2873–2911, 2000.
- [26] Kristoffer Gryte, Richard Hann, Mushfiqul Alam, Jan Rohac, Tor Arne Johansen, and Thor I. Fossen. Aerodynamic modeling of the Skywalker X8 Fixed-Wing Unmanned Aerial Vehicle. *2018 International Conference on Unmanned Aircraft Systems, ICUAS 2018*, pages 826–835, 2018.
- [27] ANSYS Inc. ANSYS FENSAP-ICE User Manual. Technical report, 2017.
- [28] Pascal Tran, Guido Barruzi, Frederic Tremblay, Wagdi Habashi, Perry Petersen, Mark Ligget, Jan Vos, Pascal Benquet, and Stefano Fiorucci. FENSAP-ICE Applications to Unmanned Aerial Vehicles (UAV). (January), 2013.
- [29] C. W. Hirt, A. A. Amsden, and J. L. Cook. An arbitrary Lagrangian-Eulerian computing method for all flow speeds. *Journal of Computational Physics*, 14(3):227–253, 1974.
- [30] Randal W Beard and Timothy W McLain. Small Unmanned Aircraft – Chapter 4: Forces and Moments. In *Small Unmanned Aircraft – Theory and Practice*. Princeton University Press, 2012.
- [31] Jan Roskam. *Airplane Flight Dynamics and Automatic Flight Controls - Part I*. DARcorporation, Lawrence, KS, 3rd editio edition, 2001.
- [32] A Deperrois. About XFLR5 calculations and experimental measurements. Technical Report October, 2009.
- [33] A Deperrois. Theoretical limitations and shortcomings of XLFR5. Technical Report June, 2019.
- [34] Maria M Seron, Tor Arne Johansen, José A De Doná, and Andrea Cristofaro. Detection and Estimation of Icing in Unmanned Aerial Vehicles using a Bank of Unknown Input Observers. pages 1–28, 2015.